





**Emulation of spin-orbit coupling for solitons in nonlinear optical media**Huangang Li (李华刚)<sup>1</sup>, Xing Zhu (朱兴)<sup>1</sup>, Boris A. Malomed,<sup>2</sup> Dumitru Mihalache<sup>3</sup>,  
Yingji He (何影记)<sup>1</sup> and Zhiwei Shi (石智伟)<sup>4,\*</sup><sup>1</sup>*School of Photoelectric Engineering, Guangdong Polytechnic Normal University, Guangzhou 510665, China*<sup>2</sup>*Department of Physical Electronics, School of Electrical Engineering, Faculty of Engineering, and Center for Light-Matter Interaction, Tel Aviv University, 69978 Tel Aviv, Israel*<sup>3</sup>*Department of Theoretical Physics, Horia Hulubei National Institute for Physics and Nuclear Engineering, Reactorulul 30, RO-077125, P.O. Box MG-6, Bucharest-Magurele, Romania*<sup>4</sup>*School of Electro-mechanical Engineering, Guangdong University of Technology, Guangzhou 510006, China*

(Received 22 January 2020; accepted 15 April 2020; published 5 May 2020)

We design a framework based on the spatial-domain copropagation of two light beams with mutually orthogonal polarizations and opposite transverse components of carrier wave vectors in a nonlinear waveguide with randomly varying birefringence, the averaging with respect to which introduces an effective Manakov nonlinearity in the system. The corresponding two-component system of nonlinear Schrödinger equations is derived, being similar to the system of coupled one-dimensional Gross-Pitaevskii equations for a binary spin-orbit-coupled Bose-Einstein condensate. The system may also include an effective Rabi coupling (direct linear mixing of the components) and a periodic potential, representing a photonic-crystal structure in the underlying waveguide. For self-focusing and self-defocusing signs of nonlinearity, soliton solutions of several symmetry types are obtained by means of numerical methods, and their stability is investigated, including gap solitons in the case when the periodic potential is present.

DOI: [10.1103/PhysRevA.101.053816](https://doi.org/10.1103/PhysRevA.101.053816)**I. INTRODUCTION AND THE MODEL**

Ultracold bosonic gases provide a versatile platform for simulating many fundamental phenomena originating in quantum optics and condensed-matter physics [1,2]. A milestone result in this direction was the experimental implementation of the (pseudo) spin-orbit coupling (SOC) and synthetic gauge fields in atomic gases [3]. The emulation of the SOC of the Dresselhaus [4] and Rashba [5] types, which play the fundamental role in the physics of semiconductors, was implemented in two-component Bose-Einstein condensates (BECs), under the action of a specially designed laser-illumination pattern. The implementation was performed by mapping the spinor wave functions of electrons in the semiconductor material into the two-component bosonic wave function of the binary condensate, so that the Hamiltonian of the bosonic gas is made tantamount to the Rashba-Dresselhaus Hamiltonians [6,7]. The realization of SOC, synthetic gauge fields [8–11], and various topological phases [12–14] in ultracold bosonic gases opens up a new field in atomic and low-temperature physics, offering powerful methods for reproducing, in a “pristine” form, various effects that were originally known in other areas, in quite complex contexts.

In BEC, nonlinearity originates from interactions between atoms. In the case of repulsive or attractive interactions, the respective mean-field Gross-Pitaevskii (GP) equations [15–17] give rise to dark [18] and band-gap [19,20] solitons or bright ones [21], respectively (localized band-gap modes are

supported by the interplay of the repulsive nonlinearity and a spatially periodic potential). While SOC in BEC is, by itself, a linear effect, it is natural to consider the interplay of SOC with the intrinsic BEC’s nonlinearity. In many theoretical works, a great variety of modes were predicted in such settings, including dark [22,23], band-gap [24,25] and bright solitons [26–29], Dirac monopoles [30], skyrmions [31], vortices [32] and vortex lattices [33], and others; see also [34] for a brief review.

The realm of photonics also offers various options for emulating basic effects known in other areas of physics. In particular, the similarity between GP equations and the nonlinear Schrödinger (NLS) equation governing the paraxial propagation of waves in optics suggests various possibilities for emulation of matter-wave effects by optical ones and vice versa [35]. In this vein, a counterpart of the remarkable mechanism of the stabilization of two-dimensional (2D) solitons in binary BEC with the attractive intrinsic nonlinearity, provided by SOC [28,29], may be applied to spatiotemporal “light bullets” in dual-core planar optical waveguides with intrinsic self-focusing [36]. In the latter case, the role of SOC terms is played by the temporal dispersion of the linear intercore coupling.

This work aims to develop an optical framework for simulating SOC effects known in pseudospinor BEC. To this end, we consider copropagation of two orthogonally polarized optical beams in a self-focusing waveguide with randomly varying birefringence. Thus, the electric constituent of the electromagnetic field is taken as

$$\mathbf{E}(x, z, t) = (1/2)[\mathbf{e}_x E_x(x, z, t) + \mathbf{e}_y E_y(x, z, t)] + \text{c.c.}, \quad (1)$$

\*szwstar@gdut.edu.cn

where  $\mathbf{e}_{x,y}$  are unit vectors transverse to the propagation axis  $z$ ,  $E_x$  and  $E_y$  being complex amplitudes of the respective field components, while  $x$  is the transverse coordinate in the waveguide,  $t$  is time, and c.c. stands for the complex-conjugate contribution. The birefringence of the medium is accounted for by the respective values of the linear refractive index,  $n_{0x} = n_0 + \delta n(z) + \Delta n$  and  $n_{0y} = n_0 - \delta n(z) - \Delta n$ , where  $\Delta n$  is a constant part of the birefringence, and  $\delta n(z)$  represents the above-mentioned term, varying as a random function of  $z$ . Further, the field components in Eq. (1) are written as

$$\begin{aligned} E_x &= A_x \exp(ik_z z + ik_x x - i\omega t), \\ E_y &= A_y \exp(ik_z z - ik_x x - i\omega t), \end{aligned} \quad (2)$$

assuming opposite signs of transverse components  $\pm k_x$  of their wave vectors, which are related to the carrier wavelength,  $\sqrt{k_z^2 + k_x^2} = 2\pi n_0/\lambda$ ,  $\omega$  being the respective frequency. In the usual paraxial approximation [37], and applying averaging with respect to the randomly varying  $\delta n(z)$ , which casts the nonlinearity in Manakov's form [34,38], that is,  $\delta n(z)$  is transformed into the self-phase modulation effect and the cross-phase modulation effect, the coupled NLS equations for slowly varying amplitudes  $A_{x,y}$  from Eqs. (1) and (2) are obtained in the following form:

$$\begin{aligned} 2ik_z \frac{dA_x}{dz} + 2ik_x \frac{\partial A_x}{\partial x} + \frac{\partial^2 A_x}{\partial x^2} + 2k_0^2 n_0 \Delta n A_x \\ + 2k_0^2 n_0 n_2 (|A_x|^2 + |A_y|^2) A_x &= 0, \\ 2ik_z \frac{dA_y}{dz} - 2ik_x \frac{\partial A_y}{\partial x} + \frac{\partial^2 A_y}{\partial x^2} - 2k_0^2 n_0 \Delta n A_y \\ + 2k_0^2 n_0 n_2 (|A_x|^2 + |A_y|^2) A_y &= 0, \end{aligned} \quad (3)$$

where  $n_2$  is the Kerr coefficient. Next, defining  $Q^\pm = (A_x \pm iA_y)/\sqrt{2}$ , Eq. (3) is transformed into a system with linear couplings between the components, represented by the fields and their first  $x$  derivatives:

$$\begin{aligned} 2ik_z \frac{dQ^+}{dz} + 2ik_x \frac{\partial Q^+}{\partial x} + \frac{\partial^2 Q^+}{\partial x^2} \\ + 2k_0^2 n_0 \Delta n Q^- + 2k_0^2 n_0 n_2 (|Q^+|^2 + |Q^-|^2) Q^+ &= 0, \\ 2ik_z \frac{dQ^-}{dz} + 2ik_x \frac{\partial Q^-}{\partial x} + \frac{\partial^2 Q^-}{\partial x^2} \\ + 2k_0^2 n_0 \Delta n Q^+ + 2k_0^2 n_0 n_2 (|Q^+|^2 + |Q^-|^2) Q^- &= 0. \end{aligned} \quad (4)$$

Next, introducing normalized variables,  $q^+ = w_0 k_0 \sqrt{n_0 n_2} Q^+$ ,  $q^- = w_0 k_0 \sqrt{n_0 n_2} Q^-$  and  $\xi = x/w_0$ ,  $\zeta = z/(k_x w_0^2)$ , where  $w_0$  is a scale factor, we arrive at the final form of the NLS system,

$$\begin{aligned} i \frac{dq^+}{d\zeta} + i\alpha \frac{\partial q^+}{\partial \xi} + \frac{1}{2} \frac{\partial^2 q^+}{\partial \xi^2} + \rho q^- + g(|q^+|^2 + |q^-|^2) q^+ &= 0, \\ i \frac{dq^-}{d\zeta} + i\alpha \frac{\partial q^-}{\partial \xi} + \frac{1}{2} \frac{\partial^2 q^-}{\partial \xi^2} + \rho q^+ + g(|q^-|^2 + |q^+|^2) q^- &= 0, \end{aligned} \quad (5)$$

where  $g = +1$  and  $-1$  correspond to the self-focusing and self-defocusing media, respectively. The constants are  $\alpha = k_x w_0$  and  $\rho = k_0^2 w_0^2 n_0 \Delta n$ . By means of additional scaling, it is possible to fix  $\alpha = 1$  in Eq. (5), but it is more convenient

to keep  $\alpha$  as a free parameter, which measures the effective SOC strength in the system. System (5) admits an obvious reduction to a single NLS equation for complex field  $q(\xi, \zeta)$  by substituting

$$q^\pm = \pm q^- = \frac{1}{\sqrt{2}} \exp \left[ i \left( -\frac{1}{2} \alpha^2 \pm \rho \right) \zeta \mp i \alpha x \right] q(\xi, \zeta). \quad (6)$$

The NLS system (5) may be used for the optical emulation of SOC in the 1D setting because, in the case of  $\rho = 0$ , it is similar to the GP equations for the SOC system [24–27,39–43]. However, Zeeman terms, in the form of  $\pm \Omega q^\pm$ , with real constant  $\Omega$ , in the equations for  $q^\pm$ , which are often included in SOC models, do not appear in the present system. In particular, the spatially periodic potential, which is added to the present system [see Eq. (13) below], was introduced differently, viz., as a Zeeman lattice, in Ref. [24].

Although the Zeeman term is absent in this model, the effect of the additional linear term  $\sim \rho$  is the same as that of the Zeeman term in the band-gap structure of the system, and it can also be derived from Eq. (3). So,  $\sim \rho$  may affect the topology of the structure, but we do not consider the topological properties of the structure here.  $\sim \rho$  in Eq. (5) may be interpreted as an emulation of the Rabi coupling in the spinor BEC system, which was introduced in Refs. [42,43]. In this connection, it is relevant to mention that the SOC-Rabi system that was introduced in Ref. [43] is written, in terms of the present notation, as

$$\begin{aligned} i \frac{dq^+}{d\zeta} + \lambda \frac{\partial q^-}{\partial \xi} + \frac{1}{2} \frac{\partial^2 q^+}{\partial \xi^2} + \rho q^- + (|q^+|^2 + |q^-|^2) q^+ &= 0, \\ i \frac{dq^-}{d\zeta} - \lambda \frac{\partial q^+}{\partial \xi} + \frac{1}{2} \frac{\partial^2 q^-}{\partial \xi^2} + \rho q^+ + (|q^-|^2 + |q^+|^2) q^- &= 0, \end{aligned} \quad (7)$$

with real coefficient  $\lambda$ . In the spinor form, the SOC operator in system (5) is  $\sigma_1 \hat{p}$ , where  $\sigma_1$  is the Pauli matrix and  $\hat{p} \equiv -i\partial_x$  is the 1D momentum operator. On the other hand, in Eq. (7) the SOC operator is  $-\sigma_2 \hat{p}$ . Unlike stationary soliton solutions found below, system (7) gives rise to shuttle motion of 1D solitons, coupled to their intrinsic oscillations [43].

In the subsequent part of the paper, we report families of solitons generated by system (5) with the self-focusing nonlinearity ( $g = 1$ ), and we address their stability in Sec. II. This is followed in Sec. III by producing soliton families in the semi-infinite and finite band gaps of the system with the focusing and defocusing nonlinearity, augmented by a spatially periodic potential. The paper is concluded in Sec. IV.

## II. SOLITONS IN HOMOGENEOUS MEDIA

The linearized version of Eq. (5) gives rise to two branches of the dispersion relation for excitations  $q^\pm \sim \exp(ib\zeta + ip\xi)$ , viz.,  $b = -(p^2/2) \pm (\alpha p + \rho)$ , where  $b$  and  $p$  are the real propagation constant and the transverse wave number, respectively. This dispersion relation contains a semi-infinite gap,  $b > b_{\max} = \alpha^2/2 + \rho$ , in which solitons may exist.

Stationary soliton solutions to Eq. (5) were sought as  $q^\pm(\xi, \zeta) = u^\pm(\xi) e^{ib\zeta}$ , where the complex functions  $u^\pm$  satisfy

the equations

$$\begin{aligned} -bu^+ + i\alpha \frac{du^-}{d\xi} + \frac{1}{2} \frac{d^2u^+}{d\xi^2} + \rho u^- + g(|u^+|^2 + |u^-|^2)u^+ &= 0, \\ -bu^- + i\alpha \frac{du^+}{d\xi} + \frac{1}{2} \frac{d^2u^-}{d\xi^2} + \rho u^+ + g(|u^-|^2 + |u^+|^2)u^- &= 0. \end{aligned} \quad (8)$$

To find localized (soliton) solutions of Eq. (8), we used the modified-squared-operator method [44]. Here, the time step  $\Delta t = 1$ . The operator  $M = cc - \partial_{\xi\xi}$ , where  $cc = 20$  denotes a constant. We chose this method because it converges quickly and can be replaced by the squared-operator method with slower convergence speed by blocking some program segments of the modified-squared-operator method near the side band. In this way, we can compare the two methods to get the exact soliton solution.

When  $\rho = 0$ , Eq. (8) admits solutions composed of real and imaginary components  $u^+(\xi)$  and  $u^-(\xi) \equiv iv^-(\xi)$ , which are subject to conditions of spatial parity of two different types. First, these are composite states in which one component [say,  $u^+(\xi)$ ] is an even (symmetric) function of  $\xi$ , while  $u^-(\xi)$  is an odd (antisymmetric) one:

$$u^+(-\xi) = u^+(\xi), \quad v^{(-)}(-\xi) = -v^-(\xi). \quad (9)$$

Typical solutions of this type for  $\rho = 0$  are shown in Figs. 1(a) and 1(b). When  $\rho \neq 0$ , the solutions for both components are complex, as shown in Figs. 1(c) and 1(d).

A different species of solitons available in the case of  $\rho = 0$  is a state subject to the condition of the cross-symmetry:

$$u^+(-\xi) = v^-(\xi), \quad v^-(-\xi) = u^+(\xi), \quad (10)$$

cf. Ref. [45]. An example of a stable soliton of this type is shown in Figs. 1(e) and 1(f). Note that similar cross-symmetric solutions are displayed below in Fig. 5 for the system including the spatially periodic potential (13).

In the case of  $\rho \neq 0$ , soliton solutions are complex. In this case, we focus on a study of solitons obeying relation (6); see Figs. 1(c) and 1(d).

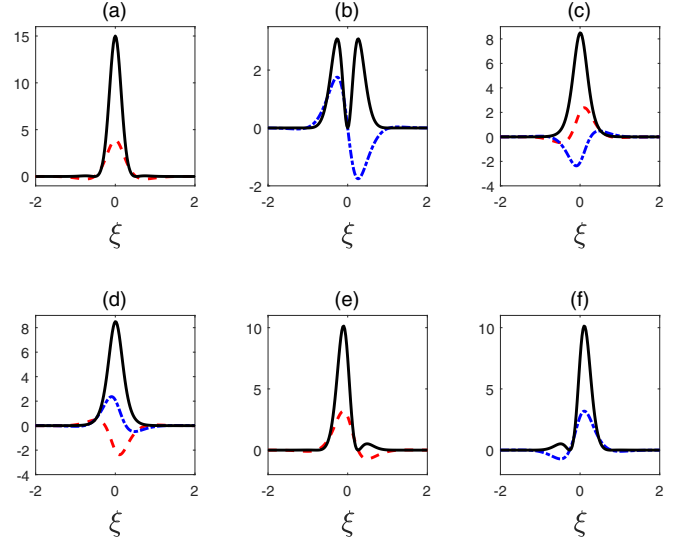


FIG. 1. Real component  $u^+$  (a) and imaginary one  $u^-$  (b) of a numerically obtained soliton solution of Eq. (8) with  $\alpha = 3$ ,  $\rho = 0$ , and  $b = 12$ . (c) and (d) Complex components of a soliton for  $\rho = 1$ , subject to constraint (6),  $q^+ = -q^-$ . (e) and (f) Real component  $u^+$  and imaginary one  $u^- \equiv iv^-$  of a cross-symmetric soliton for  $\alpha = 3$ ,  $\rho = 0$ , and  $b = 12$ , subject to constraint (10). Red dashed, blue dashed-dotted, and black solid lines display, respectively, the real part, the imaginary part, and the squared absolute value of solutions. In all cases,  $g = 1$ . All solitons displayed here are stable. All quantities are plotted in arbitrary dimensionless units.

Analysis of stability for the solitons against small perturbations was carried out by means of the standard linearization procedure. For a given stationary soliton,  $q^\pm(\xi, \zeta) = u^\pm(\xi)e^{ib\zeta}$ , small perturbations are added as  $q^\pm(\xi, \xi) = [u^\pm + \varepsilon F^\pm e^{i\delta\xi} + \varepsilon (G^\pm)^* e^{i\delta^*\xi}]e^{ib\zeta}$  with infinitesimal amplitude  $\varepsilon$ , where  $F^\pm$  and  $G^\pm$  are perturbation eigenmodes,  $\delta$  is the corresponding growth rate, and an asterisk denotes complex conjugation. The soliton is unstable if there is at least one solution with  $\text{Re}(\delta) > 0$ . Thus, the following linearized equations for small perturbations are derived from Eq. (5):

$$\begin{bmatrix} \hat{L} + g(2|u^+|^2 + |u^-|^2) & g(u^+)^2 & gu^+(u^-)^* + i\alpha \frac{\partial}{\partial x} + \rho & gu^+u^- \\ -g(u^+)^{2*} & -\hat{L} - g(2|u^+|^2 + |u^-|^2) & -g(u^+u^-)^* & -g(u^+)^*u^- + i\alpha \frac{\partial}{\partial x} - \rho \\ g(u^+)^*u^- + i\alpha \frac{\partial}{\partial x} + \rho & gu^+u^- & \hat{L} + g(|u^+|^2 + 2|u^-|^2) & g(u^-)^2 \\ -g(u^+u^-)^* & -gu^+(u^-)^* + i\alpha \frac{\partial}{\partial x} - \rho & -g(u^-)^{2*} & -\hat{L} - g(|u^+|^2 + 2|u^-|^2) \end{bmatrix} \begin{pmatrix} F^+ \\ G^+ \\ F^- \\ G^- \end{pmatrix} = -i\delta \begin{pmatrix} F^+ \\ G^+ \\ F^- \\ G^- \end{pmatrix}, \quad (11)$$

where  $\hat{L} \equiv (1/2)\partial^2/\partial x^2 - b$ . Equation (11) can be numerically solved by means of the Fourier collocation method [46,47]. This method is equivalent to equal-length linear convolution with values of the middle part, and since this method always takes an odd number of numerical points, the program design of linear convolution conversion to matrix multiplication becomes relatively simple. The method is very reliable because it is equivalent to the operation of linear convolution. Numerical results demonstrate that the solitons may

be stable both for  $\rho = 0$  and for  $\rho = 1$  [note that, although the system admits exact soliton solutions produced by substitution (6), the stability of such solutions against small perturbations breaking relations  $q^+ = \pm q^-$  is not guaranteed].

The dependence of the soliton's total power,

$$P = P_+ + P_-,$$

$$\text{where } P_\pm = \int_{-\infty}^{+\infty} |u^\pm(\xi)|^2 d\xi, \quad (12)$$

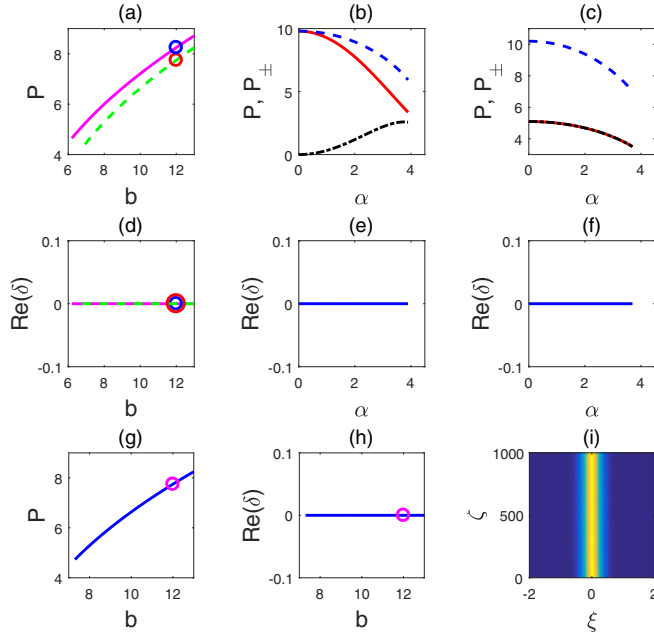


FIG. 2. (a) The total power  $P$  vs the propagation constant  $b$  for  $\alpha = 3$  in Eq. (8). The green dashed and magenta curves are plotted, respectively, for  $\rho = 0$  and 1 [recall that  $\rho$  is the coefficient of the effective Rabi coupling in Eq. (5)], the red and blue circles corresponding to the solitons shown in Figs. 1(a) and 1(b) and Figs. 1(c) and 1(d), respectively. Dependences of the powers of each component,  $P^+$ ,  $P^-$ , and the total power,  $P$  (red solid, black dashed-dotted, and blue dashed lines, respectively) on SOC strength  $\alpha$  are displayed in panel (b) for  $\rho = 0$ , and in (c) for  $\rho = 1$ , at a fixed propagation constant,  $b = 12$ . (d) The instability growth rate,  $\text{Re}(\delta)$ , vs the propagation constant,  $b$ , corresponding to (a). Dashed green and magenta lines are plotted, respectively, for  $\rho = 0$  and 1. (e) and (f) The instability growth rate,  $\text{Re}(\delta)$ , vs the SOC strength,  $\alpha$ , corresponding to (b) and (c), respectively. (g) The total power  $P$  vs propagation constant  $b$  of the cross-symmetric soliton solutions for  $\alpha = 3$  in Eq. (8). (h) The instability growth rate,  $\text{Re}(\delta)$ , vs the propagation constant,  $b$ , corresponding to (g). The magenta circles correspond to the soliton shown in Figs. 1(e) and 1(f). (i) Results of direct simulations, displayed by means of the spatiotemporal distribution of the total density,  $|q^+|^2 + |q^-|^2$ , of the evolution of the soliton, which is displayed in Figs. 1(e) and 1(f), with random-noise perturbations added at the 5% amplitude level. In all cases,  $g = 1$  (the self-focusing nonlinearity). All quantities are plotted in arbitrary dimensionless units.

on the propagation constant,  $b$ , represents a monotonically increasing function; see Fig. 2(a). It is worth noting that this dependence meets the well-known necessary stability condition, viz., the Vakhitov-Kokolov criterion,  $dP/db > 0$  [48–50]. Note also that the power of the solitons with  $\rho = 1$  is larger than that for their counterpart with the same  $b$  and  $\rho = 0$ .

Further, the dependence of the soliton's power on SOC strength  $\alpha$  is displayed in Figs. 2(b) and 2(c), which demonstrate that the solitons exist at values of  $\alpha$  below a threshold level, viz.,  $\alpha^{(\text{thr})} = 3.9$  for  $\rho = 0$  and  $\alpha^{(\text{thr})} = 3.7$  for  $\rho = 1$ . Above the threshold, the nonlinear self-focusing effect cannot balance the SOC-driven walk-off and diffraction of the two components.

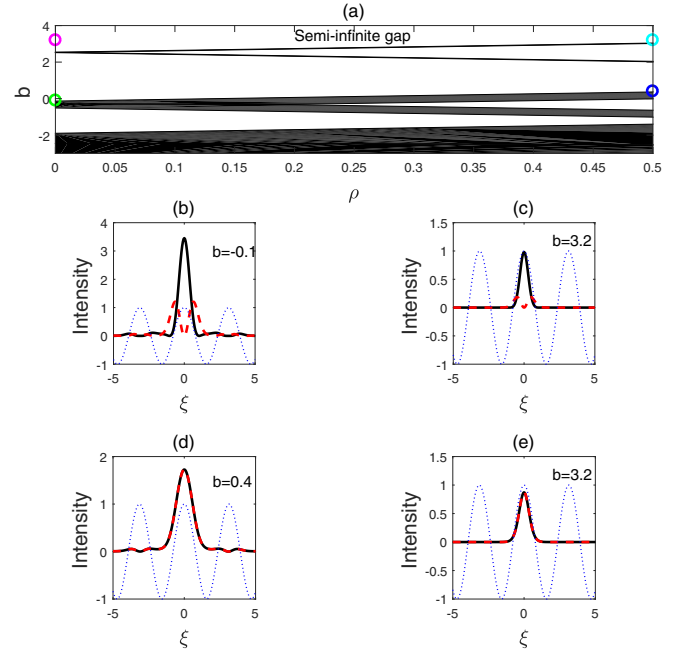


FIG. 3. (a) The evolution of the band structure (black) of the linearized system, including periodic potential (13), with the increase of the Rabi-coupling strength,  $\rho$ . Here  $b$  is the propagation constant. Green, magenta, blue, and cyan circles correspond to the solitons shown in panels (b)–(e), respectively, by means of intensity profiles  $|u^+(\xi)|^2$  and  $|u^-(\xi)|^2$  of the two components (black solid and red dashed lines, respectively): (b)  $g = -1$ ,  $b = -0.1$ , and  $\rho = 0$ ; (c)  $g = 1$ ,  $b = 3.2$ , and  $\rho = 0$ ; (d)  $g = -1$ ,  $b = 0.4$ , and  $\rho = 0.5$ ; and (e)  $g = 1$ ,  $b = 3.2$ , and  $\rho = 0.5$ . In the cases of the self-focusing and self-defocusing nonlinearity, i.e.,  $g = 1$  and  $-1$ , respectively, the displayed solitons belong to the semi-infinite and finite band gaps, respectively. In all panels, the SOC strength is  $\alpha = 1.5$ . All quantities are plotted in arbitrary dimensionless units.

We have performed the linear-stability analysis for the solitons based on Eq. (11). The results presented in Figs. 2(d)–2(f) demonstrate that the solitons are stable in the region where they exist. For the cross-symmetric soliton solutions, such as the one displayed in Figs. 1(e) and 1(f), we show the dependence of the total power  $P$  and the instability growth rate  $\text{Re}(\delta)$  on the propagation constant  $b$  in Figs. 2(g) and 2(h), respectively. This soliton family is stable, too. We have checked the robustness of this soliton species by simulating its evolution with the addition of 5% random-noise perturbations. The results, illustrated by Fig. 2(i), corroborate the stability predicted by the linear-stability analysis.

### III. GAP SOLITONS IN THE PERIODIC POTENTIAL

The existence and stability of gap solitons was studied in the presence of a periodic potential,

$$V(\xi) = 3 \cos(2\xi), \quad (13)$$

added to both equations in system (5), with the amplitude of the potential scaled to 3. The potential, which emulates the effect of an optical lattice in BEC, may be induced by the photonic-crystal structure of the underlying waveguide [51].

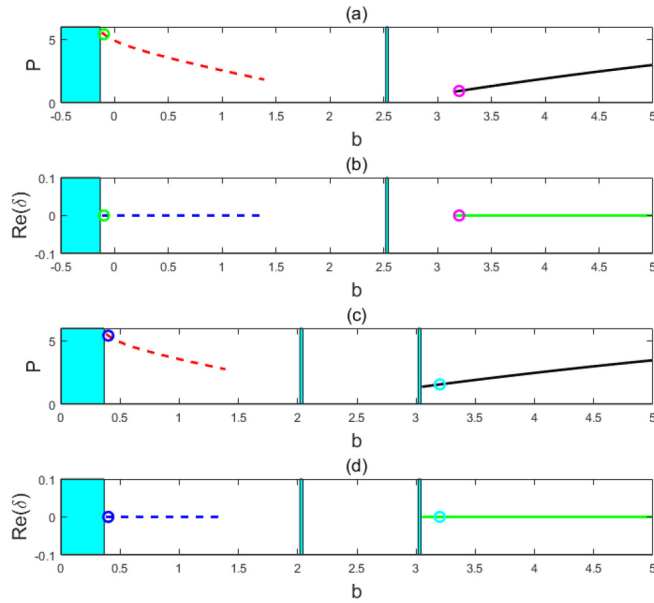


FIG. 4. The total power,  $P$  [see Eq. (12)], and the instability growth rate,  $\text{Re}(\delta)$ , vs the propagation constant,  $b$ , for solitons found in the semi-infinite and finite band gaps (right and left/central boxes, with  $g = 1$  and  $-1$ , respectively) of the system including lattice potential (13), with the Rabi-coupling constant  $\rho = 0$  in (a), (b) and  $\rho = 0.5$  in (c), (d). In all panels,  $\text{Re}(\delta) \equiv 0$  implies that all the soliton families are completely stable ( $\delta$  is the instability growth rate). Green, magenta, blue, and cyan circles represent the solitons shown in Figs. 3(b)–3(e), respectively. In all cases, the SOC strength is  $\alpha = 1.5$ . All quantities are plotted in arbitrary dimensionless units.

For SOC strength  $\alpha = 1.5$ , the band-gap structure of the linearized version of system (5), including periodic potential (13), is shown in Fig. 3(a) as a function of the Rabi-coupling strength,  $\rho$ , which strongly affects the structure. In particular, the first and second bands split into two subbands at some critical values of  $\rho$ .

When  $\rho = 0$ , two typical solitons, found in the presence of the lattice in the finite band gap and the semi-infinite one, are shown, respectively, in Fig. 3(c) for  $g = -1$  and  $b = -0.1$ , and Fig. 3(d) for  $g = 1$  and  $b = 3.2$ . These solitons are similar to those produced by Eqs. (5) with the self-focusing nonlinearity ( $g = 1$ ) in the free space (without the lattice potential), in the sense that their components  $u^+$  and  $u^-$  are pure real and imaginary ones, subject to the parity constraint (9). When  $\rho = 0.5$ , typical solitons, satisfying the same relation as in the free space,  $q^+ = \pm q^-$  [cf. Eq. (6)], are shown in Figs. 3(d) and 3(e), respectively, for the self-defocusing and self-focusing signs of the nonlinearity

Results for the solitons found in the band gaps are summarized in Fig. 4. First, Fig. 4(a) demonstrates that the solitons exist only in the above-mentioned semi-infinite gap for  $g = 1$  (self-focusing), and in the first band gap for  $g = -1$  (self-defocusing) at  $\rho = 0$ , being completely stable in their existence regions, as shown in Fig. 4(b). Further, Fig. 4(c) shows that, at  $\rho = 0.5$  (in the presence of the Rabi coupling), the solitons are again found in the semi-infinite gap at  $g = 1$ . At the same value of  $\rho = 0.5$  and with  $g = -1$ , solitons do not exist in the first band gap, but they are found in the second one.

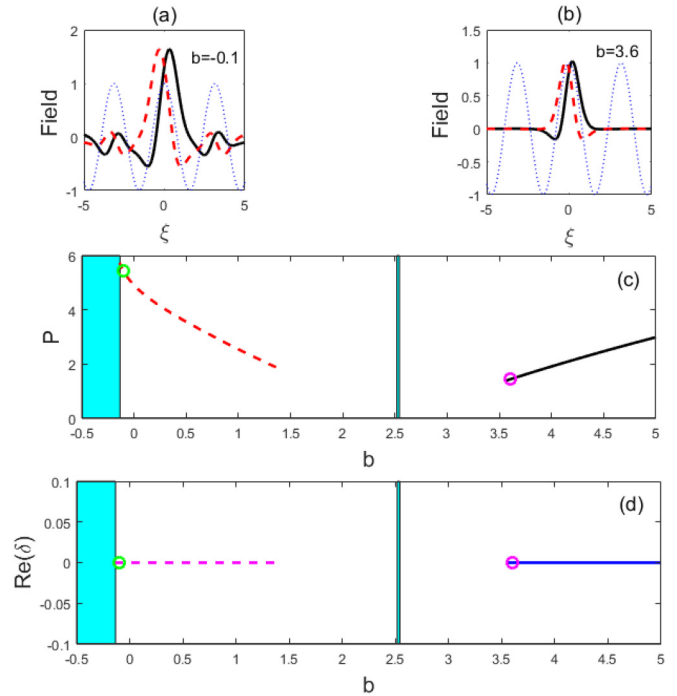


FIG. 5. Profiles of the pure real and imaginary components,  $u^+$  and  $u^- \equiv iv^-$ , of solitons produced by Eq. (8), including potential terms (13), are displayed, respectively, by black solid and red dashed lines in panels (a) for  $g = -1$ ,  $b = -0.1$ ,  $\rho = 0$ , and (b) for  $g = 1$ ,  $b = 3.6$ ,  $\rho = 0$ . (c) The total power,  $P$  [defined as per Eq. (12)], vs the propagation constant,  $b$ , for solitons found in the semi-infinite (right) and finite (left) band gaps of the system including the lattice potential (13), without the Rabi-coupling constant ( $\rho = 0$ ). (d) The instability growth rate,  $\text{Re}(\delta)$ , vs the propagation constant,  $b$ , corresponding to (c). All solitons displayed in this figure satisfy the cross-symmetry constraint (10). All quantities are plotted in arbitrary dimensionless units.

These solitons are also completely stable in their existence region, as shown in Fig. 4(d).

Finally, in the case of  $\rho = 0$  we address solitons with pure real and imaginary components obeying the cross-symmetry relation (10). Equation (8), augmented by potential term (13), produces such solitons belonging to the semi-infinite and finite band gaps, which are shown, respectively, in Figs. 5(a) and 5(b). Families of the solitons are presented by means of the respective  $P(b)$  curves in Fig. 5(c). The results of the linear-stability analysis, displayed in Fig. 5(d), demonstrate that the solitons are stable in their existence region.

#### IV. CONCLUSION

We have derived the beam-propagation equations for bimodal optical beams propagating in a nonlinear waveguide with randomly varying birefringence and a photonic-crystal structure. The averaging with respect to the randomness naturally casts the nonlinearity of the effective system in Manakov's form. The resulting equations may emulate one-dimensional SOC phenomenology in a nonlinear binary BEC, both in free space and in an optical-lattice potential. The effective SOC interaction between the copropagating beams,

which correspond to the two components of the mean-field wave function in the binary BEC, is induced by opposite transverse components of their wave vectors. Numerical results produce families of stable solitons in free space with focusing nonlinearity and in the presence of the spatially periodic potential for both focusing and defocusing signs of the nonlinearity.

As an extension of this work, it may be interesting to develop our framework for the spatial-domain propagation of light in the same setting but with two transverse coordinates, as well as for spatiotemporal propagation, which may help to emulate two-dimensional matter-wave solitons [28,32–

34,36,43] and matter-wave topological edge states [52–54] in an optical setting.

#### ACKNOWLEDGMENTS

This work was supported by the Natural Science Foundation of Guangdong Province of China (Grants No. 2016A030313747, No. 2017A030311025, and No. 2020A1515010623) and the National Natural Science Foundation of China (Grants No. 11547212 and No. 61675001). The work of B.A.M. is supported in part by the Israel Science Foundation via Grant No. 1287/17.

- 
- [1] P. Hauke, F. M. Cucchietti, L. Tagliacozzo, I. Deutsch, and M. Lewenstein, Can one trust quantum simulators? *Rep. Prog. Phys.* **75**, 082401 (2012).
- [2] T. H. Johnson, S. R. Clark, and D. Jaksch, What is a quantum simulator? *EPJ Quant. Technol.* **1**, 10 (2014).
- [3] Y.-J. Lin, K. Jimenez-Garcia, and I. B. Spielman, Spin-orbit-coupled Bose-Einstein condensates, *Nature (London)* **471**, 83 (2011).
- [4] G. Dresselhaus, Spin-orbit coupling effects in zinc blende structures, *Phys. Rev.* **100**, 580 (1955).
- [5] Y. A. Bychkov and E. I. Rashba, Oscillatory effects and the magnetic susceptibility of carriers in inversion layers, *J. Phys. C* **17**, 6039 (1984).
- [6] V. Galitski and I. B. Spielman, Spin-orbit coupling in quantum gases, *Nature (London)* **494**, 49 (2013).
- [7] H. Zhai, Degenerate quantum gases with spin-orbit coupling: A review, *Rep. Prog. Phys.* **78**, 026001 (2015).
- [8] N. Goldman, G. Juzeliūnas, P. Öhberg, and I. B. Spielman, Light-induced gauge fields for ultracold atoms, *Rep. Prog. Phys.* **77**, 126401 (2014).
- [9] E. Zohar, J. I. Cirac, and B. Reznik, Quantum simulations of lattice gauge theories using ultracold atoms in optical lattices, *Rep. Prog. Phys.* **79**, 014401 (2016).
- [10] M. Aidelsburger, Artificial gauge fields and topology with ultracold atoms in optical lattices, *J. Phys. B* **51**, 193001 (2018).
- [11] V. Galitski, G. Juzeliūnas, and I. B. Spielman, Artificial gauge fields with ultracold atoms, *Phys. Today* **72**(1), 38 (2019).
- [12] N. Goldman, J. C. Budich, and P. Zoller, Topological quantum matter with ultracold gases in optical lattices, *Nat. Phys.* **12**, 639 (2016).
- [13] N. R. Cooper, T. C. M. Group, J. Dalibard, and I. B. Spielman, Topological bands for ultracold atoms, *Rev. Mod. Phys.* **91**, 015005 (2019).
- [14] D.-W. Zhang, Y.-Q. Zhu, Y. X. Zhao, H. Yan, and S.-L. Zhu, Topological quantum matter with cold atoms, *Adv. Phys.* **67**, 253 (2019).
- [15] L. P. Pitaevskii and S. Stringari, *Bose-Einstein Condensation* (Oxford University Press, Oxford, UK, 2003).
- [16] V. S. Bagnato, D. J. Frantzeskakis, P. G. Kevrekidis, B. A. Malomed, and D. Mihalache, Bose-Einstein condensation: Twenty years after, *Rom. Rep. Phys.* **67**, 5 (2015).
- [17] B. A. Malomed and D. Mihalache, Nonlinear waves in optical and matter-wave media: A topical survey of recent theoretical and experimental results, *Rom. J. Phys.* **64**, 106 (2019).
- [18] D. J. Frantzeskakis, Dark solitons in atomic Bose-Einstein condensates: from theory to experiments, *J. Phys. A* **43**, 213001 (2010).
- [19] V. A. Brazhnyi and V. V. Konotop, Theory of nonlinear matter waves in optical lattices, *Mod. Phys. Lett. B* **18**, 627 (2004).
- [20] O. Morsch and M. Oberthaler, Dynamics of Bose-Einstein condensates in optical lattices, *Rev. Mod. Phys.* **78**, 179 (2006).
- [21] L. Salasnich, Bright solitons in ultracold atoms, *Opt. Quant. Electron.* **49**, 409 (2017).
- [22] O. Fialko, J. Brand, and U. Zülicke, Soliton magnetization dynamics in spin-orbit-coupled Bose-Einstein condensates, *Phys. Rev. A* **85**, 051605(R) (2012).
- [23] V. Achilleos, J. Stockhofe, P. G. Kevrekidis, D. J. Frantzeskakis, and P. Schmelcher, Matter-wave dark solitons and their excitation spectra in spin-orbit coupled Bose-Einstein condensates, *Europhys. Lett.* **103**, 20002 (2013).
- [24] Y. V. Kartashov, V. V. Konotop, and F. Kh. Abdullaev, Gap Solitons in a Spin-Orbit-Coupled Bose-Einstein Condensate, *Phys. Rev. Lett.* **111**, 060402 (2013).
- [25] V. E. Lobanov, Y. V. Kartashov, and V. V. Konotop, Fundamental, Multipole, and Half-Vortex Gap Solitons in Spin-Orbit Coupled Bose-Einstein Condensates, *Phys. Rev. Lett.* **112**, 180403 (2014).
- [26] V. Achilleos, D. J. Frantzeskakis, P. G. Kevrekidis, and D. E. Pelinovsky, Matter-Wave Bright Solitons in Spin-Orbit Coupled Bose-Einstein Condensates, *Phys. Rev. Lett.* **110**, 264101 (2013).
- [27] Y. Xu, Y. Zhang, and B. Wu, Bright solitons in spin-orbit-coupled Bose-Einstein condensates, *Phys. Rev. A* **87**, 013614 (2013).
- [28] H. Sakaguchi, B. Li, E. Ya. Sherman, and B. A. Malomed, Composite solitons in two-dimensional spin-orbit coupled self-attractive Bose-Einstein condensates in free space, *Rom. Rep. Phys.* **70**, 502 (2018).
- [29] Y. V. Kartashov, L. Torner, M. Modugno, E. Ya. Sherman, B. A. Malomed, and V. V. Konotop, Multidimensional hybrid Bose-Einstein condensates stabilized by lower-dimensional spin-orbit coupling, *Phys. Rev. Res.* **2**, 013036 (2020).
- [30] G. J. Conduit, Line of Dirac monopoles embedded in a Bose-Einstein condensate, *Phys. Rev. A* **86**, 021605(R) (2012).

- [31] C.-J. Wu, I. Mondragon-Shem, and X.-F. Zhou, Unconventional Bose-Einstein condensations from spin-orbit coupling, *Chin. Phys. Lett.* **28**, 097102 (2011).
- [32] B. A. Malomed, (INVITED) Vortex solitons: Old results and new perspectives, *Physica D* **399**, 108 (2019).
- [33] H. Sakaguchi and B. Li, Vortex lattice solutions to the Gross-Pitaevskii equation with spin-orbit coupling in optical lattices, *Phys. Rev. A* **87**, 015602 (2013).
- [34] B. A. Malomed, Creating solitons by means of spin-orbit coupling, *Europhys. Lett.* **122**, 36001 (2018).
- [35] C. Noh and D. G. Angelakis, Quantum simulations and many-body physics with light, *Rep. Progr. Phys.* **80**, 016401 (2017).
- [36] Y. V. Kartashov, B. A. Malomed, V. V. Konotop, V. E. Lobanov, and L. Torner, Stabilization of spatiotemporal solitons in Kerr media by dispersive coupling, *Opt. Lett.* **40**, 1045 (2015).
- [37] Y. S. Kivshar and G. P. Agrawal, *Optical Solitons: From Fibers to Photonic Crystals* (Academic, San Diego, 2003).
- [38] P. K. A. Wai, C. R. Menyuk, and H. H. Chen, Stability of solitons in randomly varying birefringent fibers, *Opt. Lett.* **16**, 1231 (1991).
- [39] X. Zhu, H. Li, Z. Shi, Y. Xiang, and Y. He, Gap solitons in spin-orbit-coupled Bose-Einstein condensates in mixed linear-nonlinear optical lattices, *J. Phys. B* **50**, 155004 (2017).
- [40] Y. V. Kartashov, V. V. Konotop, M. Modugno, and E. Ya. Sherman, Solitons in Inhomogeneous Gauge Potentials: Integrable and Nonintegrable Dynamics, *Phys. Rev. Lett.* **122**, 064101 (2019).
- [41] D. Ma and C. Jia, Soliton oscillation driven by spin-orbit coupling in spinor condensates, *Phys. Rev. A* **100**, 023629 (2019).
- [42] L. Salasnich and B. A. Malomed, Localized modes in dense repulsive and attractive Bose-Einstein condensates with spin-orbit and Rabi couplings, *Phys. Rev. A* **87**, 063625 (2013).
- [43] H. Sakaguchi and B. A. Malomed, Flipping-shuttle oscillations of bright one- and two-dimensional solitons in spin-orbit-coupled Bose-Einstein condensates with Rabi mixing, *Phys. Rev. A* **96**, 043620 (2017).
- [44] J. Yang and T. I. Lakoba, Universally-convergent squared-operator iteration methods for solitary waves in general nonlinear wave equations, *Stud. Appl. Math.* **118**, 153 (2007).
- [45] T. Mayteevarunyoo and B. A. Malomed, Skew-symmetric vortices and solitons in crossed-lattice potentials, *J. Opt. A* **11**, 094015 (2009).
- [46] J. Yang, *Nonlinear Waves in Integrable and Nonintegrable Systems* (SIAM, Philadelphia, 2010).
- [47] D. Gottlieb and S. A. Orszag, *Numerical Analysis of Spectral Methods: Theory and Applications* (SIAM, Philadelphia, 1977).
- [48] N. G. Vakhitov and A. A. Kolokolov, Stationary solutions of the wave equation in a medium with nonlinearity saturation, *Radiophys. Quantum Electron.* **16**, 783 (1973).
- [49] L. Bergé, Wave collapse in physics: principles and applications to light and plasma waves, *Phys. Rep.* **303**, 259 (1998).
- [50] G. Fibich, *The Nonlinear Schrödinger Equation: Singular Solutions and Optical Collapse* (Springer, Heidelberg, 2015).
- [51] J. D. Joannopoulos, S. G. Johnson, J. N. Winn, and R. D. Meade, *Photonic Crystals: Molding the Flow of Light* (Princeton University Press, Princeton, 2008).
- [52] C. Li, F. Ye, X. Chen, Y. Kartashov, L. Torner, and V. Konotop, Topological edge states in Rashba-Dresselhaus spin-orbit-coupled atoms in a Zeeman lattice, *Phys. Rev. A* **98**, 061601(R) (2018).
- [53] C. Li, F. Ye, Y. Kartashov, V. Konotop, and X. Chen, Localization-delocalization transition in spin-orbit-coupled Bose-Einstein condensate, *Sci. Rep.* **6**, 31700 (2016).
- [54] W. Zhang, X. Chen, Y. Kartashov, V. Konotop, and F. Ye, Coupling of Edge States and Topological Bragg Solitons, *Phys. Rev. Lett.* **123**, 254109 (2019).